Published in final edited form as:

Cell Rep. 2021 September 21; 36(12): 109751. doi:10.1016/j.celrep.2021.109751.

Kainate receptors regulate the functional properties of young adult-born dentate granule cells

Yiwen Zhu[1], **John N. Armstrong**[1], **Anis Contractor**[1,2,3,*]

[1]Department of Neuroscience, Northwestern University Feinberg School of Medicine, Chicago, IL 60611, USA

[2]Department of Neurobiology, Northwestern University, Chicago, IL 60611, USA

[3]Lead contact

SUMMARY

Both inhibitory and excitatory neurotransmitter receptors can influence maturation and survival of adult-born neurons in the dentate gyrus; nevertheless, how these two neurotransmitter systems affect integration of new neurons into the existing circuitry is still not fully characterized. Here, we demonstrate that glutamate receptors of the kainate receptor (KAR) subfamily are expressed in adult-born dentate granule cells (abDGCs) and that, through their interaction with GABAergic signaling mechanisms, they alter the functional properties of adult-born cells during a critical period of their development. Both the intrinsic properties and synaptic connectivity of young abDGCs were affected. Timed KAR loss in a cohort of young adult-born neurons in mice disrupted their performance in a spatial discrimination task but not in a hippocampal-dependent fear conditioning task. Together, these results demonstrate the importance of KARs in the proper functional development of young abDGCs.

In brief

Zhu et al. record from birth-dated, adult-born granule cells in the hippocampus to determine how their properties are affected by KARs. Both the synaptic and intrinsic membrane properties are disrupted during a short developmental window, and mice with a loss of KARs in young neurons have impairments in spatial discrimination.

Graphical Abstract

*Correspondence: a-contractor@northwestern.edu.

AUTHOR CONTRIBUTIONS

Y.Z., J.N.A., and A.C. designed the study, analyzed the data, interpreted the results, and wrote and edited the manuscript. Y.Z. performed electrophysiological recordings and behavioral experiments. J.N.A. performed the immunohistochemical experiments. A.C. obtained support for the study. All authors approved the final version of the manuscript.

DECLARATION OF INTERESTS

The authors declare no competing interests.

SUPPLEMENTAL INFORMATION

Supplemental information can be found online at https://doi.org/10.1016/j.celrep.2021.109751.

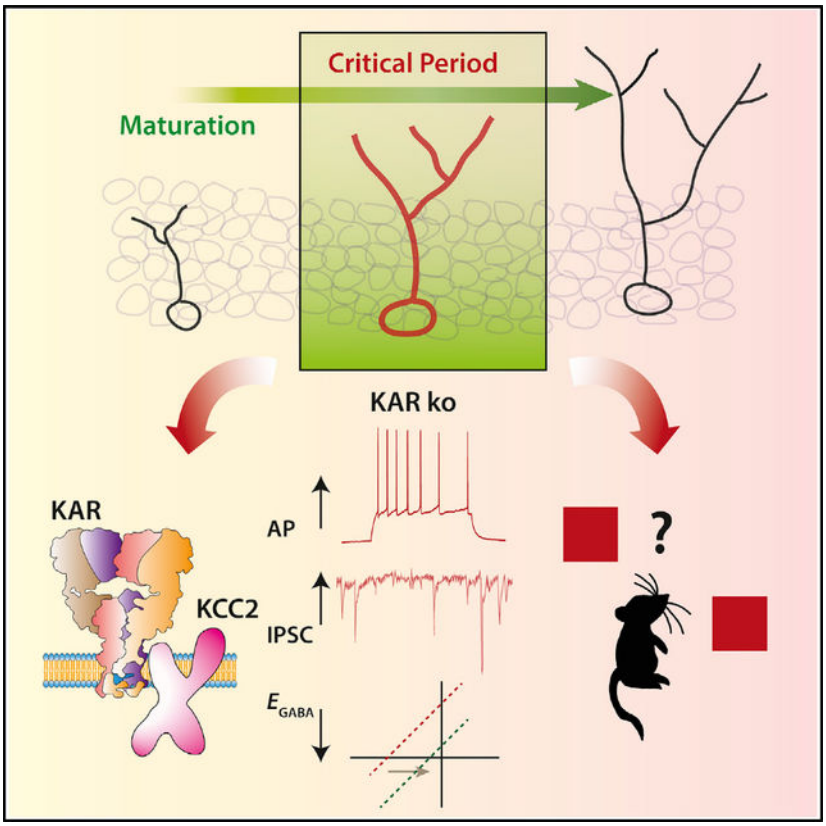

INTRODUCTION

Adult neurogenesis in the mammalian hippocampus is a structural, circuit-level brain plasticity that is mediated by the continuous generation of newborn dentate granule cells (DGCs) in the neurogenic niche in the subgranular zone (SGZ) and their incorporation into the existing hippocampal network (Gage, 2019; Ming and Song, 2011). Adult neurogenesis has been described in many mammalian species, including humans (Kempermann et al., 2018), and persists throughout life, although it is much more robust in younger brains (Kuhn et al., 1996; Moreno-Jiménez et al., 2019) and is influenced by both activity (van Praag et al., 1999) and environment (Kempermann et al., 1997). Previous studies have demonstrated that these adult-born dentate granule cells (abDGCs) have privileged roles in many hippocampal-dependent processes, including memory formation (Shors et al., 2001), consolidation (Kumar et al., 2020), and retrieval (Gu et al., 2012), pattern separation (Nakashiba et al., 2012; Sahay et al., 2011), as well as anti-depressive-like behaviors in rodents (Tunc-Ozcan et al., 2019). AbDGCs exhibit similar differentiation stages compared with developmentally born neurons (Espósito et al., 2005), and they eventually become functionally indistinguishable from the mature DGC population (Laplagne et al., 2006; van Praag et al., 2002). However, as abDGCs develop, they go through distinct phases of maturity that make them functionally separate from the surrounding mature DGCs. For example, immature DGCs exhibit elevated excitability and plasticity compared with mature DGCs during a critical time window (Ge et al., 2007; Schmidt-Hieber et al., 2004). They

also form inhibitory and excitatory synaptic connections as they mature, and both their intrinsic properties and the strength of their synaptic innervation (Dieni et al., 2013a, 2016) are important for their engagement in the hippocampal circuit that potentially provides unique contributions to the function of the adult hippocampus (Tuncdemir et al., 2019). Thus, the mechanisms that control the duration of abDGC immaturity can influence their functional properties and, in turn, their effect on hippocampal circuit function.

Maturation of adult-born neurons has been demonstrated to be activity dependent and can be regulated by both intrinsic excitability and network activity. For example, manipulations that increase or decrease the intrinsic excitability of abDGCs can result in their accelerated or delayed maturation, respectively (Piatti et al., 2011; Sim et al., 2013). Network activity in the hippocampal environment is sensed by maturing abDGCs through its developing synaptic connectivity, and both GABA and glutamate signaling have important roles in regulating the maturation of newborn neurons. AbDGCs initially receive GABAergic input, which, up to around 2 weeks after differentiation, is depolarizing because of a relatively high internal cellular chloride ($[Cl^-]_{int}$) concentration (Dieni et al., 2013b; Ge et al., 2006). Disruption of this early depolarizing GABA signaling by targeting the chloride transporters, which regulate intracellular chloride homeostasis, delays the dendritic maturation of abDGCs (Ge et al., 2006). Depolarizing GABA in abDGCs is also required for unsilencing of N-methyl d-aspartate receptor (NMDAR)-only synapses (Chancey et al., 2013), whereas NMDAR signaling increases the survival rate of abDGCs and regulates dendritic morphology (Mu et al., 2015; Tashiro et al., 2006a). Little is known about the role of non-NMDA receptors, especially kainate receptors (KARs), in any of the aspects of neurogenesis in the adult dentate gyrus. KARs are of particular interest because they have multiple roles in synaptic and neuronal development in developmentally born neurons (Jack et al., 2019; Lauri et al., 2006; Orav et al., 2017; Sakha et al., 2016). In particular, it has been demonstrated that the functional and morphological maturation of mossy fiber synapses formed by developmentally born granule cells is delayed in GluK2$^{-/-}$ mice (Lanore et al., 2012). Moreover, antagonists of KARs applied to neuroblasts in the subventricular zone increase their migration speed (Platel et al., 2008), and low concentrations of non-NMDA receptor agonists increase proliferation and differentiation of neural progenitors in the hippocampus (Pérez-Gómez and Tasker, 2012). In addition, behavioral studies in KAR-mutant mice have demonstrated a disruption in affective-like behaviors (Aller et al., 2015; Catches et al., 2012), which can also be correlated with altered adult hippocampal neurogenesis (Anacker et al., 2018; Snyder et al., 2011). Given that, we tested whether KARs have functional roles in abDGCs in the hippocampus. We found that KARs are expressed in young abDGCs with the GluK2 KAR subunit the principal obligatory subunit. Single-cell knockout of GluK2 and retroviral birth-dating of abDGCs were used to determine the functional properties of abDGCs at early maturation time points. Both the intrinsic neuronal properties and synaptic connectivity during an early critical postmitotic period suggested that the functional development of abDGCs was accelerated in the absence of KARs, because of an effect on the GABA reversal potential in developing newborn neurons. Using an inducible strategy to time the knockout of GluK2 in a cohort of abDGCs, we found that loss of GluK2 in young neurons during this critical period caused deficits in mice in tests that require spatial discrimination but no major disruption in a

conditioned-fear test. These results demonstrate a previously unknown role for KARs in regulating the functional properties of abDGCs during a critical period in their development, which further exemplifies the importance of KARs to hippocampal function.

RESULTS

Young abDGCs display KAR-mediated currents

To follow the development and maturation of abDGCs we used a retroviral labeling strategy which allows dividing cells in the SGZ to be selectively labeled and accurately birth-dated (Tashiro et al., 2006b). Injection into the SGZ of a retrovirus packaged with GFP (RV-GFP) or red fluorescent protein (RFP; RV-RFP) or GFP-IRES-Cre (RV-GFPCre) under a CAG promoter resulted in fluorescent birth-dated abDGCs that could be visualized and targeted for patch clamp recordings at various days post-injection (dpi) in acute slices (Figures 1A and 1B) (Tashiro et al., 2006a, 2006b). KAR subunits are amply expressed in the dentate gyrus (Bureau et al., 1999) but as in many other neuronal types they are not localized and available at synapses under normal conditions (Epsztein et al., 2005). However, it is not known whether newly generated DGCs also express KARs during early postmitotic development. We first determined that KAR-mediated currents are present on developing abDGCs in wild-type mice by recording from virally labeled neurons in the dentate and applying the KAR agonist domoate (10 μM) in the presence of antagonists of AMPA (GYKI 52466, 50 μM), NMDA (D-APV, 50 μM), and GABA (bicuculline, 10 μM) receptors. We found that domoate elicited a small KAR-mediated current in most of the recordings from 14 dpi labeled abDGCs and increasingly larger currents in almost all 21 dpi and 28 dpi labeled abDGCs (Figure 1C). In comparison, domoate-induced currents were completely eliminated in all recorded neurons (21–28 dpi) in constitutive GluK2$^{-/-}$ (knockout [KO]) mice indicating that the GluK2 subunit is the primary obligatory KAR subunit expressed in abDGCs (Figures 1C and 1D). In line with that, we also found that, in recordings from abDGCs in mice in which the auxiliary KAR subunit GluK4 is ablated (Catches et al., 2012; Fernandes et al., 2009), there was no difference in the amplitude of the domoate elicited current (GluK4 KO 21 dpi: 28.9 ± 7.1 pA, n = 10; wild type [WT] 21 dpi: 27.4 ± 6.5 pA, n = 9). To determine whether a conditional KO strategy for GluK2 would, likewise, eliminate KAR-mediated currents selectively in birth-dated abDGCs, we injected RV-RFP and RV-GFPCre retroviruses into the SGZ of each hemisphere in floxed *Grik2* (*Grik2*f/f) mice (Marshall et al., 2018) to compare both GluK2 cKO (RV-GFPCre) and control (RV-RFP) abDGCs (Figures 1A and 1B). We recorded domoate-induced currents and validated that RV-mediated transduction caused the specific ablation of functional KARs in Cre-expressing GFP^{+} abDGCs at all the analyzed time points: 14, 21, 28, and 42 dpi (Figures 1E and 1F). In recordings from unlabeled DGCs located distal to the SGZ in the GC layer, we observed domoate-induced currents of similar amplitude to those in 42 dpi abDGCs (Figure 1E). Taken together, these results demonstrate that KARs that contain the GluK2 subunit are expressed during early postmitotic development of abDGCs in the adult hippocampus.

Passive and active membrane properties of young abDGCs during an early critical period are disrupted by ablation of GluK2

To determine whether loss of KARs affects abDGC properties, we measured several morpho-functional parameters of maturation in GluK2 conditional KO (cKO) neurons during a critical period for their development at 14–42 dpi (Ge et al., 2007; Tashiro et al., 2007). As demonstrated previously (Mongiat et al., 2009), young neurons possess high input resistance (R_{in}), which decreased as they matured over time (Figure 2A). However, we found that the R_{in} of GluK2 cKO abDGCs was significantly lower in 21 dpi, young abDGCs in comparison to the control neurons (Figure 2A). In recordings from birth-dated abDGCs in constitutive GluK2 KO mice, we saw an even more-pronounced effect with significantly lower R_{in} of GluK2 KO neurons at both 21 dpi and 28 dpi (Figure S1A), demonstrating that this cell-autonomous effect of the loss of GluK2 is reproducible across different KO models. The R_{in} of developing abDGCs is a prime indicator of the maturity of the neurons (Schmidt-Hieber et al., 2004; Trinchero et al., 2019); thus, the lower R_{in} measured in 21 dpi GluK2 cKO abDGCs demonstrates that, surprisingly, loss of GluK2 results in abDGCs with the intrinsic property of more mature, newborn neurons. In constitutive GluK2 KO mice, we also measured the resting membrane potential (RMP) of abDGCs, which became more hyperpolarized at increasing postmitotic times, but we did not observe a genotype-dependent effect on this parameter (Figure S1B). Newborn neurons also mature in their ability to fire repetitive action potentials (APs) when their intrinsic conductance changes during development. We, therefore, measured the AP firing capacity of birth-dated abDGCs in response to supra-threshold, current-step injections. In particular, at 21 dpi, GluK2 cKO neurons supported the firing of more APs in response to increasing current, whereas control neurons of the same postmitotic age fired only approximately five APs, on average, at the highest current injection (Figures 2C and 2D). This effect on AP firing properties was pronounced at 21 dpi, and no difference was observed in more mature neurons at 28 dpi (Figures 2E and 2F). This also correlated with a difference in the measured rheobase in cKO neurons at 21 dpi (Figure 2B). Elevated firing is surprising given the lower R_{in} of 21 dpi GluK2 cKO abDGCs compared with controls but likely reflects the elevated expression of sodium and potassium conductance that young abDGCs display during later stages of their development (Espósito et al., 2005). Consistent with these findings in cKO neurons, birth-dated abDGCs recorded in constitutive GluK2 KO mice also had the same altered AP response to current injection during this early critical period (Figures S1C–S1E).

As a measure of the morphological development of abDGCs, the total dendritic length was measured at several postmitotic time points in both constitutive GluK2 KO mice and cKO neurons. There was a clear increase in dendritic length in abDGCs between 14 dpi and at later postmitotic times, with a marked increase between 14 dpi and 21 dpi (Figure 3B). However, there was no difference in total dendritic length when GluK2 was ablated (cKO, Figures 3A and 3B; GluK2 KO, Figures S2A–S2C) or in the number of branch points (Figures 3C and S2D). As an alternate measure of morphological transformation of maturing abDGCs, we also classified the localization of neurons in the SGZ and GC layers (Espósito et al., 2005). To label neurons and time the ablation of GluK2 in a larger population of abDGCs, we used a genetic strategy involving the use of the tamoxifen (TAM)-inducible $Ascl1^{CreERT2}$ mouse (Yang et al., 2015) crossed to the Ai9 allele (Ascl1tdTom) and

GluK2f/f alleles (Ascl1cKO). Quantifying the localization of tdTom-labeled neurons in the SGZ and three radially spaced zones of the GC layers (Z1 to Z3) (Figure 3E) (Espósito et al., 2005) in Ascl1tdTom and Ascl1cKO mice indicated there was no difference in the localization of abDGCs 21 days after TAM administration in the cohort with GluK2 ablated (Figures 3D and 3E). In addition, the percentage of $tdTom^+$ neurons that were positive for doublecortin (DCX), a marker for young abDGCs (Brown et al., 2003) was not different in Ascl1tdTom and Ascl1cKO mice (Figures 3D and 3F).

Taken together, ablation of GluK2 has a cell-autonomous effect on the development of the functional, intrinsic properties of young newborn abDGCs and results in more-mature AP firing properties during a short postmitotic time window 3 weeks after birth. Conversely, there was no observed effect at 21 dpi on the morphological properties that mature in tandem with the electro physiological properties of abDGCs. This apparent selective effect on the functional properties suggests that GluK2-containing KARs normally regulate abDGC functional maturation during an early developmental period.

GABAergic synaptic events are elevated in 21 dpi GluK2 cKO abDGCs

Because the intrinsic and AP firing properties of abDGCs are altered after GluK2 KO during the period when synaptic connections are being formed (Ge et al., 2006), we determined the consequences of GluK2 ablation on abDGC integration into the circuit by recording GABAergic and glutamatergic postsynaptic events in both GluK2 KO mice and GluK2 cKO adult-born neurons. Recordings from 21 dpi neurons demonstrated that there was no difference in the frequency or amplitude of spontaneous excitatory postsynaptic currents (sEPSCs) either in GluK2 KO mice or in GluK2 cKO abDGCs (Figure S3). In separate recordings of inhibitory synaptic events, the frequency of spontaneous inhibitory postsynaptic currents (sIPSCs) was elevated in 21 dpi GluK2 cKO abDGCs; no difference was observed in sIPSC frequency in 28 dpi or older cKO abDGCs (Figures 4A and 4C). Analysis of the amplitudes of sIPSCs demonstrated there was also an increase in the mean sIPSC amplitude in cKO neurons specifically at 21 dpi but not at other times after injection (Figures 4B and 4C). Cumulative probability plots of sIPSC inter-event interval and amplitude also confirmed that 21 dpi GluK2 cKO abDGCs had elevated numbers of sIPSC events as well as larger sIPSC amplitudes than control abDGCs had (Figures 4D and 4E). A similar increase in sIPSC frequency was also found in birth-dated 21 dpi abDGCs in recordings from GluK2 KO mice (Figures S4A and S4C). Together these data demonstrate that there is a specific increase in spontaneous inhibitory events in 21 dpi abDGCs that is likely due to an increase in the number of inhibitory synaptic contacts made onto GluK2 cKO neurons at a critical period of development. The efficacy of individual synapses was not affected, and there was no clear increase in release probability of inhibitory synapses as measured by mIPSC frequency at 21 dpi (data not shown).

GluK2 cKO abDGCs demonstrate a more depolarized E_{GABA} at 21 dpi

Our findings to this point are consistent with altered functional properties of 21 dpi abDGCs during a critical time of development, suggesting that GluK2 KARs in abDGCs have a powerful role in the development of newborn neurons. One way that GluK2 may affect abDGC maturation is through its known effects on GABA, which, in turn, can have a

trophic effect on abDGCs (Catavero et al., 2018; Ge et al., 2006). During early development of abDGCs, GABA is depolarizing because of the relatively high intracellular chloride concentration $[Cl^-]_{int}$, which results in a depolarized reversal potential for GABA (E_{GABA}) (Ge et al., 2006). $[Cl^-]_{int}$ is developmentally regulated by the Cl^- cotransporters, and disrupting Cl^- homeostasis in abDGCs alters formation of its synaptic connections (Ge et al., 2006). KARs can exist in a complex with the K^+-Cl^- cotransporter KCC2, and loss of KARs from this complex in hippocampal neurons leads to a reduction in KCC2 surface expression and a depolarization of E_{GABA} (Mahadevan et al., 2014). Therefore, we asked whether loss of GluK2 could potentially disrupt Cl^- homeostasis and result in a more depolarized E_{GABA} in developing abDGCs. Gramicidin perforated patch recordings were used to measure GABA-evoked currents in abDGCs at 14, 21, and 28 dpi, when E_{GABA} is progressively maturing to more hyperpolarized values (Ge et al., 2006). In control recordings (RV-RFP), there was a significant shift in E_{GABA} to more hyperpolarized values between 14 dpi and 21 dpi (Figure 5C). However, in GluK2 cKO neurons, E_{GABA} remained depolarized at 21 dpi and was significantly depolarized compared with recordings from control abDGCs (Figures 5). Similar perforated patch recordings of GABA currents from GluK2 KO mice demonstrated that, in 21 dpi, birth-dated abDGCs, E_{GABA} was consistently more depolarized than in recordings from WT neurons (Figure S5). In both the cKO and constitutive GluK2 KO mice, E_{GABA} recorded from 28 dpi abDGCs was normal (Figures 5C and S5B). Together these data demonstrate that, during an early critical period of abDGC development, GluK2 receptors are required for the normal hyperpolarizing switch in E_{GABA} that occurs between 14 dpi and 21 dpi, at a time when NKCC1 and KCC2 expression is changing reciprocally (Ge et al., 2006) and when synaptic input to abDGCs switches from primarily GABAergic to supporting both excitatory and inhibitory synapses (Espósito et al., 2005).

Spatial discrimination is impaired 21 days after cKO of GluK2 in abDGCs

Young abDGCs are thought to have privileged roles in the hippocampus, stemming from the unique and evolving functional properties that make them particularly important for certain cognitive tasks (Gonçalves et al., 2016). In particular, tasks that require discrimination of similar objects or situations are proposed to involve the activity of abDGCs (Johnston et al., 2016; Nakashiba et al., 2012), and ablation of abDGCs can impair mice in tasks that require discrimination of similar patterns (Clelland et al., 2009). In contrast, ablation of GluK2 in abDGCs produces a relatively specific change in the functional properties of abDGCs during a brief window in their development. To determine whether GluK2 KO in abDGCs affects relevant hippocampal-dependent behaviors, we investigated the consequences of specifically ablating GluK2 receptors in a cohort of abDGCs. We crossed the TAM-inducible $Ascl1^{CreERT2}$ mice with the *Grik2*f/f mice to time the ablation of GluK2 restricted to a cohort of abDGCs (Yang et al., 2015). Because Cre recombinase is activated by TAM in both type 1 and type 2 cells in the neurogenic niche, it has been predicted that recombination occurs in a large population of neurons generated at the time of TAM administration (derived from type 2 fast amplifying progenitors), followed by recombination in younger cohorts (derived from the type 1 slowly dividing stem cells) (Yang et al., 2015). Therefore, for TAM administration started 21 days before behavioral analysis, GluK2 Ascl1cKO occurred in 21-day-old and younger postmitotic abDGCs (Figure 6A).

Ascl1^{CreERT2} mice crossed to reporter mice had clear labeling of abDGCs, which were largely distributed in L1 of the GC layer, with some neurons showing clear morphology of young abDGCs (Figure 6B). Cell counts did not demonstrate any difference in the number of labeled neurons between Ascl1tdTom and Ascl1cKO mice (Figure 6C). Exploratory behavior of mice was analyzed in a task in which they discriminate between novel and familiar spatial locations to determine whether cKO of GluK2 in that cohort of abDGCs affects their performance. Prior work has established that spatial discrimination in mice is dependent upon the DG and that manipulation of adult neurogenesis disrupts spatial discrimination (Castillon et al., 2018; Clelland et al., 2009; Goodman et al., 2010; Laszczyk et al., 2017; Marschallinger et al., 2015). Mice were habituated for 3 consecutive days before training on the first day of the test (object location memory [OLM] training), which occurred 21 days after TAM induction (Figure 6A). During OLM training, mice explored for a 10-min period, at will, in a chamber in which two identical objects were placed at two set locations (Figure 6D). Mice were returned to the chamber 24 h after OLM training for OLM testing. During OLM testing, the location of one of the objects was moved to a new position, and mice were allowed to freely explore in the same chamber during a 5-min session (Figure 6E). The discrimination index was calculated to reflect the exploratory preference of the mice for the novel object location. Although control mice (Ascl1tdTom) had a clear preference for the object moved to a new location, mice in which GluK2 had been ablated in the 21-day-old and younger cohort of abDGCs (Ascl1cKO) demonstrated no preference (Figure 6F). The total exploration time for both object locations during training and testing sessions (Figures 6G and 6H), as well as the total distance traveled during OLM testing (Figure 6I) were the same between Ascl1tdTom and Ascl1cKO animals

In a further test of whether there were more general disruptions in behaviors that require hippocampal activity but not specifically the DG or abDGCs, we tested mice in trace fear conditioning (Chowdhury et al., 2005). On day 21–23 after TAM induction, mice were conditioned with three pairings of a conditioned stimulus (CS; tone) and an unconditioned stimulus (US; foot shock) (Figures S6A and S6B). On the subsequent day, mice were tested for contextual fear in the same chamber and separately for CS freezing in a novel context (Figure S6C). In each case, there was no difference in freezing behaviors either during acquisition or testing, suggesting that cKO of GluK2 in a cohort of young abDGCs does not have a general effect on hippocampal-dependent memory tasks.

DISCUSSION

How abDGCs develop and integrate into the hippocampal network is of considerable interest because there are numerous studies that have demonstrated that young adult-born neurons have unique functional properties that imbue them with distinct roles in hippocampal function (Gonçalves et al., 2016). Neuronal activity driven through the action of the neurotransmitters GABA and glutamate are of primary relevance to the maturation of postmitotic neurons in the DG (Chancey et al., 2013; Duveau et al., 2011; Ge et al., 2006; Piatti et al., 2011; Toni and Schinder, 2015). AbDGCs are initially innervated by GABA inputs during the first and second postmitotic week (Espósito et al., 2005; Groisman et al., 2020; Remmers et al., 2020), with glutamatergic synapses developing later at around the fourth postmitotic week (Espósito et al., 2005). GABA also has a non-synaptic role with a

prominent tonic $GABA_AR$ current found in newly differentiated neurons (Ge et al., 2006) as well as in neural stem cells (Song et al., 2012). Importantly, as with developmentally born neurons, abDGCs undergo a period during an early postmitotic stage in which the reversal potential for GABA is relatively depolarized and activation of $GABA_ARs$ can potentially depolarize abDGCs (Chancey et al., 2013; Ge et al., 2006). Selective knockdown of the Cl^- transporter NKCC1 in abDGCs results in a disruption of $[Cl^-]_{INT}$ homeostasis and disrupted synapse formation and dendritic growth (Ge et al., 2006). Depolarizing GABA is also critical to experience-dependent NMDAR-mediated synaptic plasticity mechanisms in abDGCs by providing the membrane depolarization required for easing Mg^{2+} block at NMDAR-only synapses (Chancey et al., 2013). Therefore, as in other developing neurons, there is an important interplay between GABA and glutamatergic signaling in developing abDGCs.

Here, we focused on the potential role that KARs may have in abDGCs. KARs are a distinct family of glutamate receptors, whose functions are both diverse and not fully realized (Carta et al., 2014; Lerma and Marques, 2013). They are primarily ionotropic receptors but can also signal through metabotropic signaling pathways at both pre- and postsynaptic sites. KARs are present in most cell types in the hippocampus but are surprisingly rare at postsynaptic sites. In the DG, the GluK2 KAR subunit is expressed at high levels, likely existing in a heteromeric complex with the high-affinity subunits (Bureau et al., 1999), and presynaptic KARs have been well characterized on the DG axons and presynaptic terminals (Contractor et al., 2000, 2001; Lauri et al., 2001; Schmitz et al., 2001). Prior work has demonstrated that the development of the DG mossy fiber axon to CA3 connection is delayed in GluK2 KO mice, establishing the importance of KARs to normal hippocampal circuit development (Lanore et al., 2012). Although there are KARs on the somatodendritic membrane of mature DGCs, KARs are not present at postsynaptic sites under normal conditions (Epsztein et al., 2005). There has been no prior work on KARs on abDGCs, and it was unknown whether and when they are present in early postmitotic developing abDGCs. Functional KARs were previously described in DCX^+ neuroblasts in the lateral ventricle (Platel et al., 2008). Using birth-dating and labeling of developing abDGCs, we found that KARs containing the GluK2 subunit are functionally expressed by abDGCs at early postmitotic times. This raised an important question about their roles, given that they are present at times when there are no, or very sparse, glutamatergic synapses present on abDGCs, and moreover, KARs are not localized to synaptic sites. We adopted a conditional single-cell KO approach to birth date and record from cKO neurons. We also recorded from birth-dated abDGCs in a constitutive KO mouse model. Surprisingly, we found multiple functional consequences of the loss of GluK2 at the earliest postmitotic time points during what has been defined as a critical period for development of abDGCs (Chancey et al., 2013; Kitamura et al., 2010; Tashiro et al., 2007). Specifically, at 21 dpi, the R_{in} of GluK2 cKO abDGCs was significantly lower and was more consistent with neurons of later postmitotic times. In line with functionally more-mature newborn neurons, 21 dpi cKO abDGCs responded to current injection with increased AP firing compared with WT neurons. Synaptic measures also strongly suggested that the 21 dpi abDGCs with GluK2 ablated had a more mature functional profile with increased frequency and elevated amplitude of sIPSCs. Although functional measures of intrinsic and synaptic properties suggested a more mature profile for KO abDGCs, there

was no correlated change in morphological parameters that are also measures of maturation. Given these specific alterations in the functional maturation of abDGCs, it is interesting to note that they seem to be separable from dendritic development, in that the disruption of one does not correlate with changes in the other.

Our study led us to examine the maturation of E_{GABA} in GluK2 cKO abDGCs. Both developmentally born and adult-born neurons are subject to trophic effects of shifts in the GABA reversal potential as the neurons mature. In abDGCs, the transition from a relatively depolarized E_{GABA} to a more hyperpolarized mature value of E_{GABA} occurs between 14 dpi and 21 dpi (Ge et al., 2006). Importantly, the GluK2 receptor subunit exists in a complex with the Cl^- extruder KCC2, which maintains lower $[Cl^-]_{INT}$ as neurons develop (Mahadevan et al., 2014). GluK2 increases the abundance of surface KCC2 (Pressey et al., 2017) and affects the maturation of spines in developmentally born hippocampal neurons (Kesaf et al., 2020). We found that, in GluK2 cKO abDGCs, the normal developmental switch from depolarizing to hyperpolarizing E_{GABA} is delayed, such that, at 21 dpi, E_{GABA} is still depolarized. A similar result was observed in birth-dated abDGCs in GluK2 KO mice. These data demonstrate that loss of KARs in abDGCs affects the GABA polarity switch during a critical time window when the abDGCs are maturing. This action of KARs in regulating the expression of KCC2 may be the prominent role they play in developing neurons, which have few or sparse glutamatergic inputs and also which, in many cases, never localize KARs to synapses at which they can be activated by synaptically released glutamate. As such, it is possible that a primary role that KARs have in abDGCs is as a non-canonical partner of the Cl^- transporter (Mahadevan et al., 2014).

Young abDGCs are of special importance to hippocampal circuits and have been proposed to have a large effect on behaviors involving the hippocampus. Newborn neurons have a particularly important role in behaviors during the critical period soon after they make contacts with other components of the DG-CA3 microcircuit. AbDGCs form functional output synapses with CA3 as early as 2 weeks postmitotic, and those connections fully mature between 21 and 28 dpi (Gu et al., 2012). It is also during the 3–4 postmitotic weeks that abDGCs are active during hippocampal-dependent learning tasks, and reversible optical silencing of 4-week-old neurons disrupts memory retrieval (Gu et al., 2012). Because loss of KARs has a selective effect on the functional properties of abDGCs during this critical time window, we tested whether conditional disruption of GluK2 affected behavior of mice. It is possible that the functional changes in abDGCs during this time cause cumulative effects because neurons with altered properties are continuously added to the network, producing a more dramatic change to the circuit. To ablate GluK2 in a large cohort of abDGCs, we used the $Ascl1^{CreERT2}$ mice, which allowed us to temporally and spatially restrict KO of GluK2 to the adult SGZ. Although this provided the advantage of a broader KO of GluK2, the temporal precision is less than that achieved with a retroviral approach, giving a wider range of postmitotic ages of abDGC in which GluK2 is ablated (Yang et al., 2015). We tested mice in which cKO of GluK2 had been initiated 21 days preceding a spontaneous spatial discrimination task (Dix and Aggleton, 1999). In the testing phase, the level of discrimination was significantly reduced in GluK2 cKO mice. Although it will take future studies to fully understand how the altered cellular properties of cKO abDGCs affect behavior, possibilities include that there is a delay in the downstream

connectivity to hilar and CA3 targets (Lanore et al., 2012) and also that the altered GABA reversal potential leads to increased, nonspecific activity of abDGCs, which might disrupt relevant behaviors. We also tested mice in a trace fear conditioning task, which requires involvement of hippocampal circuitry, and found no difference in the cKO mice during either acquisition or recall of fear memory. Together, these results suggest that disruption of the normal functional properties of developing abDGCs leads to selective effects on a spatial discrimination behavior but leaves other behaviors that require uncompromised functioning of the hippocampal circuits unaffected.

The roles that KARs have in circuit development and function are still not fully appreciated. This description of their roles in abDGCs during a critical time window in their development provides another important facet of their contribution to hippocampal function.

STAR✶METHODS

RESOURCE AVAILABILITY

Lead contact—Further information and requests for resources and reagents should be directed to and will be fulfilled by the lead contact, Anis Contractor (a-contractor@northwestern.edu)

Materials availability—Mouse lines generated in this study are available by direct distribution after completion of a standard MTA.

Data and code availability—All data reported in this paper will be shared by the lead contact upon request.

This paper does not report original code.

Any additional information required to reanalyze the data reported in this paper is available from the lead contact upon request.

EXPERIMENTAL MODEL AND SUBJECT DETAILS

Animals—All animal care and procedures were approved by and conducted in accordance with the Northwestern University Institutional Animal Care and Use Committee (IACUC). Mice of the same sex were group-housed with a 14 h/10 h light/dark cycle. Ascl1^{CreERT2} mice were purchased from the Jackson Laboratory, and crossed with our *Grik2*f/f; Ai9 (C57BL/6) mice (Marshall et al., 2018) to generate conditional knockout of kainate receptor subunit GluK2 in abDGCs upon tamoxifen administration. GluK2 KO mice were bred in house from animals supplied originally from Stephen Heinemann (The Salk Institute) (Mulle et al., 1998). Animals aged between 8–10 weeks of both sexes were used in experiments.

Cell lines—GP2–293 cells (a gift from Dr. John Kessler, Northwestern University, Chicago, IL) were stored in frozen aliquots and thawed and propagated in 10 cm plates before use in viral production. Cells were grown in GP2–293 media consisting of DMEM with high glucose, L-glutamine, sodium pyruvate, penicillin/streptomycin, and 10% FBS.

Plates were incubated at 37°C in 5% CO_2 until cells reached 70% confluency for passage and 90%–95% confluency for transfection as below.

METHOD DETAILS

Retroviral birth-dating—Concentrated Moloney Murine Leukemia Virus-based retroviral vectors were prepared as described (Remmers et al., 2020; Remmers and Contractor, 2018; Tashiro et al., 2006b). Briefly, GP2–293 cells were co-transfected with VSVG and CAG-GFP-IRES-CRE (Addgene plasmid # 48201), CAG-RFP, or CAG-GFP (gifts from Dr. Fred Gage, Salk Institute, La Jolla, CA) using Lipofectamine 2000 in Opti-MEM. 3 and 6 days after transfection, growth media containing retrovirus from the transfected cells was collected, filtered, and centrifuged at 25,000 rpm for 2–2.5 hours at 4°C. The precipitated viral pellet was re-suspended in phosphate-buffered saline (PBS), aliquoted, and stored at −80°C until further use. To label and birthdate abDGCs, 0.5–1.5 μL of the concentrated retroviral solution was delivered bilaterally to the subgranular zone (SGZ) of 8–10 weeks old mice via stereotaxic injection under ketamine/xylazine anesthesia as previously described (Remmers and Contractor, 2018). The following injection coordinates from bregma (in millimeters) were used: −2.0 anteroposterior, ± 1.6 mediolateral, and −2.4 dorsoventral.

Hippocampal slice electrophysiology—Mice were anesthetized with isoflurane followed by ketamine/xylazine, then rapid cardiac perfusion was performed using ice-cold sucrose artificial cerebrospinal fluid (ACSF) containing the following (in mM): 85 NaCl, 2.5 KCl, 1.25 NaH_2PO_4, 25 $NaHCO_3$, 25 glucose, 75 sucrose, 0.5 $CaCl_2$, and 4 $MgCl_2$, equilibrated with 95% O_2/5% CO_2 before mice were decapitated. Brains were rapidly removed and placed in the same ice-cold sucrose ACSF as described above. Coronal hippocampal slices (250 mm thick) were prepared using a Leica VT1000S or VT1200 S vibratome and transferred to a heated (28–32°C) holding chamber containing the same sucrose ACSF, which was gradually exchanged for regular ACSF containing the following (in mM): 125 NaCl, 2.5 KCl, 1.25 NaH_2PO_4, 25 $NaHCO_3$, 25 glucose, 2 $CaCl_2$, and 1 $MgCl_2$, equilibrated with 95% O_2/5% CO_2 at room temperature. After incubation in regular ACSF for at least one hour, slices were transferred to a recording chamber and perfused continuously with oxygenated regular ACSF at a flow rate of 2 ml/min. The dentate gyrus was visualized under DIC optics and retrovirus-labeled abDGCs were identified based on GFP or RFP reporter fluorescence.

Recording electrodes were made from borosilicate glass pipettes and had a resistance of 3.5–6.5 MΩ when filled with an internal solution containing the following (in mM): 130 K-gluconate, 10 KCl, 10 HEPES, 4 Mg-ATP, 0.3 Na-GTP, and 10 Na_2Phosphocreatine, pH adjusted to 7.3 with KOH. Input resistances were determined in whole-cell voltage-clamp mode by holding cells at −70 mV and presenting a −5 mV hyperpolarizing voltage step with a duration of 100 ms. For recordings from “mature DGCs” unlabeled cells residing in the inner two thirds of the GCL were sampled. Resting membrane potentials were measured in current-clamp mode at least 5 minutes after formation of the whole-cell recording configuration. Input-output (I/O) relationship was generated by injecting various amount of current to hold each cell’s membrane potential close to −70 mV while further injecting

0–100 pA current in 10 pA increments and counting spike number in response to each current step.

For domoate (Dom)-induced current and postsynaptic current recordings, the internal solution contained (in mM): 95 CsF, 25 CsCl, 10 HEPES, 10 EGTA, 2 NaCl, 2 Mg-ATP, 10 QX-314, 5 TEA-Cl, and 5 4AP, pH adjusted to 7.3 with CsOH, 280–290 mOsm. Kainate receptor mediated currents were induced by bath application of 10 μM Dom in the presence of 10 μM bicuculline, 50 μM GYKI, and 50 μM D-APV; or 1 μM Dom in the presence of 10 μM bicuculline, 50 μM picrotoxin, 1 μM TTX, 50 μM GYKI, and 50 μM D-APV. Spontaneous IPSCs were pharmacologically isolated by bath application of 10 μM CNQX and 50 μM D-APV, while spontaneous EPSCs were pharmacologically isolated by 10 μM bicuculline, 50 μM picrotoxin, and 50 μM D-APV. Miniature IPSCs were recorded in the additional presence of 1 μM TTX. All synaptic events were recorded between 26–30°C and analyzed using Mini Analysis Program (Synaptosoft).

For gramicidin perforated patch recordings, pipettes were filled with (in mM) 150 KCl and 10 HEPES, pH adjusted to 7.2 with Tris-OH, and gramicidin was added at a concentration of 80 μg/ml. GABAergic currents were evoked under voltage-clamp at different holding potentials (−100 to +30 mV, 10 mV step) by focal puff application of 100 mM GABA via a Picos-prizter III (50 ms duration, 2–8 psi) in the presence of 1 μM TTX, 10 μM CNQX, and 50 μM D-APV. Current-voltage relationships (I-V curve) for each cell were plotted and E_{GABA} was measured as the intersect between the x axis and the linear fit of the I-V curve. Unless otherwise stated all electrophysiological data were acquired at 10 kHz and analyzed using pClamp 10 software (Molecular Devices).

Immunohistochemistry—Mice were anesthetized with isoflurane followed by ketamine/xylazine mixture, and perfused transcardially with PBS containing 0.02% sodium nitrite, followed by 2% paraformaldehyde (PFA) in 0.1 M sodium acetate buffer (pH 6.5), then 2% PFA in 0.1 M sodium borate buffer (pH 8.5). Brains were left "*in situ*" overnight at 4°C, removed from the skull, and post-fixed for 12–16 hours in 2% PFA in 0.1 M sodium borate buffer at 4°C, then sliced using a vibrating microtome (Leica Vibratome, VT1000S). Free floating coronal sections (50 μm) were collected and stored in PBS + 0.02% sodium azide at 4°C until immunostaining. First, sections were permeabilized in 50 mM glycine containing 0.01% Triton X-100 and 0.01% NP-40 for 30 minutes, washed 3 × 15 minutes in Tris buffered saline containing 0.05% bovine serum albumin (TBS-BSA), then blocked for 1 hour in TBS-BSA containing 1% normal donkey serum (NDS; Jackson ImmunoResearch Laboratories Inc., catalog No. 017–000-121) plus unconjugated donkey anti-rabbit IgG polyclonal (1:1000; Southern Biotech., catalog No. 6411–01), unconjugated donkey anti-chicken IgY polyclonal (1:1000; Fisher Scientific, catalog No. SA172002) and unconjugated donkey anti-goat IgG polyclonal (1:1000; Southern Biotech., catalog No. 6460–01). Sections were then washed 3 × 15 minutes in TBS-BSA and incubated overnight on an orbital shaker with the primary antibodies in TBS-BSA + 0.25% NDS at room temperature (RT): rabbit polyclonal anti-RFP (1:5000; Abcam, catalog No. ab62341), goat polyclonal anti-DCX IgG (1:3000; Santa Cruz Biotechnology, Inc., catalog No. sc8066), and chicken polyclonal anti-NeuN IgY (1:5000; EMD Millipore, catalog No. ABN91). On the following day, sections were washed 3 × 15 minutes in TBS-BSA and blocked for

15 minutes in TBS-BSA + 0.25% NDS before incubation with the following secondary antibodies at RT for 1 hour: donkey anti-rabbit IgG (H & L) Alexa Fluor Plus 594 (1:1000; Thermo Fisher Scientific, catalog No. A32754), donkey anti-goat IgG (H & L) Alexa Fluor Plus 680 (1:1000; Thermo Fisher Scientific, catalog No. A32860) and donkey anti-chicken IgG (H & L) Biotin-SP (1:1000; EMD Millipore, catalog No. AP194B). Sections were then washed 3 × 15 minutes in TBS and incubated with Alexa Fluor 405 or 488 streptavidin conjugates (1:1000; Thermo Fisher Scientific, catalog No. S32351 and S32354 respectively) for another hour. Afterward, sections were washed again 3 × 15 minutes in TBS, mounted onto microscope slides, air-dried overnight and coverslipped with either FluorSave Reagent (EMD Millipore, catalog No. 345789) or ProLong Diamond Antifade (Thermo Fisher Scientific, catalog No. P36970). Finally, the coverslips were cured overnight before their edges were sealed with clear nail polish, and imaged using a Nikon A1 confocal microscope. All acquired images were adjusted for optimal brightness/contrast in ImageJ. Cell counting was performed using the ImageJ Cell Counter plugin.

For abDGC dendritic morphology reconstruction, biocytin was included in the internal solution (5 mg/ml) in the patch pipette in some recordings. After 15–30 min of dialysis, pipette was carefully withdrawn leaving the cell body intact. Slice containing the biocytin-filled abDGC was then treated with 4% PFA/PBS overnight at 4°C, washed 3 × 20 min in PBS, and blocked with 0.4% Triton X-100 plus 1% BSA and 5% NDS in PBS for one hour at RT. Slice was then incubated with streptavidin-conjugated Alexa 488 or 555 (1:500) in blocking buffer (PBS containing 1% BSA, 5% NDS and 0.2% Triton X-100) for 45 min (rocking at RT), rinsed in PBS for 3 × 5 min, and mounted in ProLong Diamond Antifade Mountant for confocal imaging. Z-stacks of all biocytin-filled abDGCs were acquired using a Nikon A1 confocal microscope, and cells with z range < 25 μm were discarded. Analysis of dendritic length and branch points were performed in Imaris software using a combination of auto-path and auto-depth filament tracing modes.

Behavioral analysis—To activate Cre-recombinase activity and test the behavioral consequences in the inducible GluK2 knock-out mice, 8–9 weeks old *Grik2*f/f;Ai9:*Ascl1*^{CreERT2} and *Grik2*$^{+/+}$;Ai9;*Ascl1*^{CreERT2} mice received daily tamoxifen I.P. injections (180 mg/kg/d, dissolved in 10% EtOH/90% sunflower seed oil) for 5 consecutive days. 21 days after TAM induction the novel object location memory (OLM) test was performed similarly to a previously published protocol (Vogel-Ciernia and Wood, 2014). Briefly, prior to OLM training, animals were habituated to handling by the experimenter 2–5 min daily for 5 days and the testing chamber (33 cm × 33 cm × 35 cm) 5 min daily for 3 days. On OLM training day (21–22 dpi), two identical objects (randomized from red cuboids, 5.5 × 5.5 × 7.5 cm; blue cuboids, 3 × 3 × 19 cm; and blue cylinders, 7.5 × 7.5 × 7.5 cm) were placed symmetrically relative to a black marking strip inside the testing chamber, and animals were allowed to freely explore both objects for 10 minutes. Mice were returned to for testing 24 hours later, when one of the objects had been moved to a novel location inside the chamber. Animals were allowed to explore both objects for 5 min. Preference for the novel object location was assessed by the discrimination index (DI) which is calculated as follows: (time exploring object at the novel location - time exploring object at the familiar location) / (time exploring novel + familiar) *100. Animals that had DI

more than ± 20 during training were considered to have a significant location bias thus were excluded from later analysis. Animal activity was video recorded and tracked and analyzed using EthoVision XT (Noldus).

Trace fear conditioning training was performed at 21–23 dpi according to a previous study (Farley et al., 2011). On the training day, animals were presented with three pairings of the CS (30 s of pulsed white noise at 5 Hz, 5 ms rise/fall, 75 dB), and a US (a 1 s, 0.7 mA scrambled shock to the cage floor). The CS and US were separated by a 20 s trace interval, and the inter-trial interval was 410 s. 24 hours later, animals were reintroduced to the original training context for 5 minutes in the absence of CS/US, and contextual fear memory was accessed by scoring freezing during the first 180 s period. Three hours later, trace fear memory was tested. Animals were placed in a novel context for 180 s, then they were presented with the CS for a duration of 60 s. Freezing percentage was calculated for a 180 s baseline (no CS) period, a 60 s CS period, and as well as a 20 s trace period immediately following the CS. All behavior was video recorded and freezing time scored automatically using Freeze Frame 4 (Actimetrics), then reviewed by the experimenter blind to the animal genotype.

QUANTIFICATION AND STATISTICAL ANALYSIS

All statistical tests were performed using Microsoft Excel and OriginPro software. For all independent comparisons, statistical significance was assessed by the nonparametric Mann-Whitney U test. For comparing multiple-trial data sets, two-way repeated ANOVA was applied. Non-parametric comparisons of the cumulative distributions of the intervals and amplitude of synaptic events were made with the Kolmogorov-Smirnov test. Differences were considered significant when $p < 0.05$. All data are reported as mean ± SEM.

Supplementary Material

Refer to Web version on PubMed Central for supplementary material.

ACKNOWLEDGMENTS

This work was supported by NIH/NIMH grant R01MH099114 and NIH/NINDS grant R01NS115471 to A.C. and a NCI Center Support Grant (NCI CA060553) to the Center for Advanced Microscopy at The Feinberg School of Medicine.

REFERENCES

Aller MI, Pecoraro V, Paternain AV, Canals S, and Lerma J (2015). Increased dosage of high-affinity kainate receptor gene *grik4* alters synaptic transmission and reproduces autism spectrum disorders features. J. Neurosci. 35, 13619–13628. [PubMed: 26446216]

Anacker C, Luna VM, Stevens GS, Millette A, Shores R, Jimenez JC, Chen B, and Hen R (2018). Hippocampal neurogenesis confers stress resilience by inhibiting the ventral dentate gyrus. Nature 559, 98–102. [PubMed: 29950730]

Brown JP, Couillard-Després S, Cooper-Kuhn CM, Winkler J, Aigner L, and Kuhn HG (2003). Transient expression of doublecortin during adult neurogenesis. J. Comp. Neurol. 467, 1–10. [PubMed: 14574675]

Bureau I, Bischoff S, Heinemann SF, and Mulle C (1999). Kainate receptor-mediated responses in the CA1 field of wild-type and GluR6-deficient mice. J. Neurosci. 19, 653–663. [PubMed: 9880586]

Carta M, Fiè vre S, Gorlewicz A, and Mulle C (2014). Kainate receptors in the hippocampus. Eur. J. Neurosci. 39, 1835–1844. [PubMed: 24738709]

Castillon C, Lunion S, Desvignes N, Hanauer A, Laroche S, and Poirier R (2018). Selective alteration of adult hippocampal neurogenesis and impaired spatial pattern separation performance in the RSK2-deficient mouse model of Coffin-Lowry syndrome. Neurobiol. Dis. 115, 69–81. [PubMed: 29627578]

Catavero C, Bao H, and Song J (2018). Neural mechanisms underlying GABAergic regulation of adult hippocampal neurogenesis. Cell Tissue Res. 371, 33–46. [PubMed: 28948349]

Catches JS, Xu J, and Contractor A (2012). Genetic ablation of the GluK4 kainate receptor subunit causes anxiolytic and antidepressant-like behavior in mice. Behav. Brain Res. 228, 406–414. [PubMed: 22203159]

Chancey JH, Adlaf EW, Sapp MC, Pugh PC, Wadiche JI, and Overstreet-Wadiche LS (2013). GABA depolarization is required for experience-dependent synapse unsilencing in adult-born neurons. J. Neurosci. 33, 6614–6622. [PubMed: 23575858]

Chowdhury N, Quinn JJ, and Fanselow MS (2005). Dorsal hippocampus involvement in trace fear conditioning with long, but not short, trace intervals in mice. Behav. Neurosci. 119, 1396–1402. [PubMed: 16300446]

Clelland CD, Choi M, Romberg C, Clemenson GD Jr., Fragniere A, Tyers P, Jessberger S, Saksida LM, Barker RA, Gage FH, and Bussey TJ (2009). A functional role for adult hippocampal neurogenesis in spatial pattern separation. Science 325, 210–213. [PubMed: 19590004]

Contractor A, Swanson GT, Sailer A, O'Gorman S, and Heinemann SF (2000). Identification of the kainate receptor subunits underlying modulation of excitatory synaptic transmission in the CA3 region of the hippocampus. J. Neurosci. 20, 8269–8278. [PubMed: 11069933]

Contractor A, Swanson G, and Heinemann SF (2001). Kainate receptors are involved in short- and long-term plasticity at mossy fiber synapses in the hippocampus. Neuron 29, 209–216. [PubMed: 11182092]

Dieni CV, Chancey JH, and Overstreet-Wadiche LS (2013a). Dynamic functions of GABA signaling during granule cell maturation. Front. Neural Circuits 6, 113. [PubMed: 23316139]

Dieni CV, Nietz AK, Panichi R, Wadiche JI, and Overstreet-Wadiche L (2013b). Distinct determinants of sparse activation during granule cell maturation. J. Neurosci. 33, 19131–19142. [PubMed: 24305810]

Dieni CV, Panichi R, Aimone JB, Kuo CT, Wadiche JI, and Overstreet-Wadiche L (2016). Low excitatory innervation balances high intrinsic excitability of immature dentate neurons. Nat. Commun. 7, 11313. [PubMed: 27095423]

Dix SL, and Aggleton JP (1999). Extending the spontaneous preference test of recognition: evidence of object-location and object-context recognition. Behav. Brain Res. 99, 191–200. [PubMed: 10512585]

Duveau V, Laustela S, Barth L, Gianolini F, Vogt KE, Keist R, Chandra D, Homanics GE, Rudolph U, and Fritschy JM (2011). Spatiotemporal specificity of GABAA receptor-mediated regulation of adult hippocampal neurogenesis. Eur. J. Neurosci. 34, 362–373. [PubMed: 21722213]

Epsztein J, Represa A, Jorquera I, Ben-Ari Y, and Crépel V (2005). Recurrent mossy fibers establish aberrant kainate receptor-operated synapses on granule cells from epileptic rats. J. Neurosci. 25, 8229–8239. [PubMed: 16148230]

Espósito MS, Piatti VC, Laplagne DA, Morgenstern NA, Ferrari CC, Pitossi FJ, and Schinder AF (2005). Neuronal differentiation in the adult hippocampus recapitulates embryonic development. J. Neurosci. 25, 10074–10086. [PubMed: 16267214]

Farley SJ, McKay BM, Disterhoft JF, and Weiss C (2011). Reevaluating hippocampus-dependent learning in FVB/N mice. Behav. Neurosci. 125, 871–878. [PubMed: 22122148]

Fernandes HB, Catches JS, Petralia RS, Copits BA, Xu J, Russell TA, Swanson GT, and Contractor A (2009). High-affinity kainate receptor subunits are necessary for ionotropic but not metabotropic signaling. Neuron 63, 818–829. [PubMed: 19778510]

Gage FH (2019). Adult neurogenesis in mammals. Science 364, 827–828. [PubMed: 31147506]

Ge S, Goh EL, Sailor KA, Kitabatake Y, Ming GL, and Song H (2006). GABA regulates synaptic integration of newly generated neurons in the adult brain. Nature 439, 589–593. [PubMed: 16341203]

Ge S, Yang CH, Hsu KS, Ming GL, and Song H (2007). A critical period for enhanced synaptic plasticity in newly generated neurons of the adult brain. Neuron 54, 559–566. [PubMed: 17521569]

Gonçalves JT, Schafer ST, and Gage FH (2016). Adult neurogenesis in the hippocampus: from stem cells to behavior. Cell 167, 897–914. [PubMed: 27814520]

Goodman T, Trouche S, Massou I, Verret L, Zerwas M, Roullet P, and Rampon C (2010). Young hippocampal neurons are critical for recent and remote spatial memory in adult mice. Neuroscience 171, 769–778. [PubMed: 20883747]

Groisman AI, Yang SM, and Schinder AF (2020). Differential coupling of adult-born granule cells to parvalbumin and somatostatin interneurons. Cell Rep. 30, 202–214.e4. [PubMed: 31914387]

Gu Y, Arruda-Carvalho M, Wang J, Janoschka SR, Josselyn SA, Frankland PW, and Ge S (2012). Optical controlling reveals time-dependent roles for adult-born dentate granule cells. Nat. Neurosci. 15, 1700–1706. [PubMed: 23143513]

Jack A, Hamad MIK, Gonda S, Gralla S, Pahl S, Hollmann M, and Wahle P (2019). Development of cortical pyramidal cell and interneuronal dendrites: a role for kainate receptor subunits and NETO1. Mol. Neurobiol. 56, 4960–4979. [PubMed: 30421168]

Johnston ST, Shtrahman M, Parylak S, Gonçalves JT, and Gage FH (2016). Paradox of pattern separation and adult neurogenesis: a dual role for new neurons balancing memory resolution and robustness. Neurobiol. Learn. Mem. 129, 60–68. [PubMed: 26549627]

Kempermann G, Kuhn HG, and Gage FH (1997). More hippocampal neurons in adult mice living in an enriched environment. Nature 386, 493–495. [PubMed: 9087407]

Kempermann G, Gage FH, Aigner L, Song H, Curtis MA, Thuret S, Kuhn HG, Jessberger S, Frankland PW, Cameron HA, et al. (2018). Human adult neurogenesis: evidence and remaining questions. Cell Stem Cell 23, 25–30. [PubMed: 29681514]

Kesaf S, Khirug S, Dinh E, Saez Garcia M, Soni S, Orav E, Delpire E, Taira T, Lauri SE, and Rivera C (2020). The kainate receptor subunit GluK2 interacts with KCC2 to promote maturation of dendritic spines. Front. Cell. Neurosci. 14, 252. [PubMed: 33005130]

Kitamura T, Saitoh Y, Murayama A, Sugiyama H, and Inokuchi K (2010). LTP induction within a narrow critical period of immature stages enhances the survival of newly generated neurons in the adult rat dentate gyrus. Mol. Brain 3, 13. [PubMed: 20426820]

Kuhn HG, Dickinson-Anson H, and Gage FH (1996). Neurogenesis in the dentate gyrus of the adult rat: age-related decrease of neuronal progenitor proliferation. J. Neurosci. 16, 2027–2033. [PubMed: 8604047]

Kumar D, Koyanagi I, Carrier-Ruiz A, Vergara P, Srinivasan S, Sugaya Y, Kasuya M, Yu TS, Vogt KE, Muratani M, et al. (2020). Sparse activity of hippocampal adult-born neurons during REM sleep is necessary for memory consolidation. Neuron 107, 552–565.e10. [PubMed: 32502462]

Lanore F, Labrousse VF, Szabo Z, Normand E, Blanchet C, and Mulle C (2012). Deficits in morphofunctional maturation of hippocampal mossy fiber synapses in a mouse model of intellectual disability. J. Neurosci. 32, 17882–17893. [PubMed: 23223307]

Laplagne DA, Espósito MS, Piatti VC, Morgenstern NA, Zhao C, van Praag H, Gage FH, and Schinder AF (2006). Functional convergence of neurons generated in the developing and adult hippocampus. PLoS Biol. 4, e409. [PubMed: 17121455]

Laszczyk AM, Fox-Quick S, Vo HT, Nettles D, Pugh PC, Overstreet-Wadiche L, and King GD (2017). Klotho regulates postnatal neurogenesis and protects against age-related spatial memory loss. Neurobiol. Aging 59, 41–54. [PubMed: 28837861]

Lauri SE, Bortolotto ZA, Bleakman D, Ornstein PL, Lodge D, Isaac JT, and Collingridge GL (2001). A critical role of a facilitatory presynaptic kainate receptor in mossy fiber LTP. Neuron 32, 697–709. [PubMed: 11719209]

Lauri SE, Vesikansa A, Segerstråle M, Collingridge GL, Isaac JT, and Taira T (2006). Functional maturation of CA1 synapses involves activity-dependent loss of tonic kainate receptor-mediated inhibition of glutamate release. Neuron 50, 415–429. [PubMed: 16675396]

Lerma J, and Marques JM (2013). Kainate receptors in health and disease. Neuron 80, 292–311. [PubMed: 24139035]

Mahadevan V, Pressey JC, Acton BA, Uvarov P, Huang MY, Chevrier J, Puchalski A, Li CM, Ivakine EA, Airaksinen MS, et al. (2014). Kainate receptors coexist in a functional complex with KCC2 and regulate chloride homeostasis in hippocampal neurons. Cell Rep. 7, 1762–1770. [PubMed: 24910435]

Marschallinger J, Sah A, Schmuckermair C, Unger M, Rotheneichner P, Kharitonova M, Waclawiczek A, Gerner P, Jaksch-Bogensperger H, Berger S, et al. (2015). The L-type calcium channel Cav1.3 is required for proper hippocampal neurogenesis and cognitive functions. Cell Calcium 58, 606–616. [PubMed: 26459417]

Marshall JJ, Xu J, and Contractor A (2018). Kainate receptors inhibit glutamate release via mobilization of endocannabinoids in striatal direct pathway spiny projection neurons. J. Neurosci. 38, 3901–3910. [PubMed: 29540547]

Ming GL, and Song H (2011). Adult neurogenesis in the mammalian brain: significant answers and significant questions. Neuron 70, 687–702. [PubMed: 21609825]

Mongiat LA, Espósito MS, Lombardi G, and Schinder AF (2009). Reliable activation of immature neurons in the adult hippocampus. PLoS ONE 4, e5320. [PubMed: 19399173]

Moreno-Jiménez EP, Flor-García M, Terreros-Roncal J, Rábano A, Cafini F, Pallas-Bazarra N, Ávila J, and Llorens-Martín M (2019). Adult hippocampal neurogenesis is abundant in neurologically healthy subjects and drops sharply in patients with Alzheimer's disease. Nat. Med. 25, 554–560. [PubMed: 30911133]

Mu Y, Zhao C, Toni N, Yao J, and Gage FH (2015). Distinct roles of NMDA receptors at different stages of granule cell development in the adult brain. eLife 4, e07871. [PubMed: 26473971]

Mulle C, Sailer A, Pérez-Otaño I, Dickinson-Anson H, Castillo PE, Bureau I, Maron C, Gage FH, Mann JR, Bettler B, and Heinemann SF (1998). Altered synaptic physiology and reduced susceptibility to kainite-induced seizures in GluR6-deficient mice. Nature 392, 601–605. [PubMed: 9580260]

Nakashiba T, Cushman JD, Pelkey KA, Renaudineau S, Buhl DL, McHugh TJ, Rodriguez Barrera V, Chittajallu R, Iwamoto KS, McBain CJ, et al. (2012). Young dentate granule cells mediate pattern separation, whereas old granule cells facilitate pattern completion. Cell 149, 188–201. [PubMed: 22365813]

Orav E, Atanasova T, Shintyapina A, Kesaf S, Kokko M, Partanen J, Taira T, and Lauri SE (2017). NETO1 guides development of glutamatergic connectivity in the hippocampus by regulating axonal kainate receptors. eNeuro 4, ENEURO.0048–17.2017.

Pérez-Gómez A, and Tasker RA (2012). Enhanced neurogenesis in organo-typic cultures of rat hippocampus after transient subfield-selective excitotoxic insult induced by domoic acid. Neuroscience 208, 97–108. [PubMed: 22366222]

Piatti VC, Davies-Sala MG, Espósito MS, Mongiat LA, Trinchero MF, and Schinder AF (2011). The timing for neuronal maturation in the adult hippocampus is modulated by local network activity. J. Neurosci. 31, 7715–7728. [PubMed: 21613484]

Platel JC, Heintz T, Young S, Gordon V, and Bordey A (2008). Tonic activation of GLUK5 kainate receptors decreases neuroblast migration in whole-mounts of the subventricular zone. J. Physiol. 586, 3783–3793. [PubMed: 18565997]

Pressey JC, Mahadevan V, Khademullah CS, Dargaei Z, Chevrier J, Ye W, Huang M, Chauhan AK, Meas SJ, Uvarov P, et al. (2017). A kainate receptor subunit promotes the recycling of the neuron-specific K^+-Cl^- co-transporter KCC2 in hippocampal neurons. J. Biol. Chem. 292, 6190–6201. [PubMed: 28235805]

Remmers CL, and Contractor A (2018). Development of GABAergic inputs is not altered in early maturation of adult born dentate granule neurons in fragile X mice. eNeuro 5, ENEURO.0137–18.2018.

Remmers CL, Castillon CCM, Armstrong JN, and Contractor A (2020). Recruitment of parvalbumin and somatostatin interneuron inputs to adult born dentate granule neurons. Sci. Rep. 10, 17522. [PubMed: 33067500]

Sahay A, Scobie KN, Hill AS, O'Carroll CM, Kheirbek MA, Burghardt NS, Fenton AA, Dranovsky A, and Hen R (2011). Increasing adult hippocampal neurogenesis is sufficient to improve pattern separation. Nature 472, 466–470. [PubMed: 21460835]

Sakha P, Vesikansa A, Orav E, Heikkinen J, Kukko-Lukjanov TK, Shintyapina A, Franssila S, Jokinen V, Huttunen HJ, and Lauri SE (2016). Axonal kainate receptors modulate the strength of efferent connectivity by regulating presynaptic differentiation. Front. Cell. Neurosci. 10, 3. [PubMed: 26834558]

Schmidt-Hieber C, Jonas P, and Bischofberger J (2004). Enhanced synaptic plasticity in newly generated granule cells of the adult hippocampus. Nature 429, 184–187. [PubMed: 15107864]

Schmitz D, Mellor J, and Nicoll RA (2001). Presynaptic kainate receptor mediation of frequency facilitation at hippocampal mossy fiber synapses. Science 291, 1972–1976. [PubMed: 11239159]

Schneider CA, Rasband WS, and Eliceiri KW (2012). NIH Image to ImageJ: 25 years of image analysis. Nat. Methods 9, 671–675. [PubMed: 22930834]

Shors TJ, Miesegaes G, Beylin A, Zhao M, Rydel T, and Gould E (2001). Neurogenesis in the adult is involved in the formation of trace memories. Nature 410, 372–376. [PubMed: 11268214]

Sim S, Antolin S, Lin CW, Lin Y, and Lois C (2013). Increased cell-intrinsic excitability induces synaptic changes in new neurons in the adult dentate gyrus that require Npas4. J. Neurosci. 33, 7928–7940. [PubMed: 23637184]

Snyder JS, Soumier A, Brewer M, Pickel J, and Cameron HA (2011). Adult hippocampal neurogenesis buffers stress responses and depressive behaviour. Nature 476, 458–461. [PubMed: 21814201]

Song J, Zhong C, Bonaguidi MA, Sun GJ, Hsu D, Gu Y, Meletis K, Huang ZJ, Ge S, Enikolopov G, et al. (2012). Neuronal circuitry mechanism regulating adult quiescent neural stem-cell fate decision. Nature 489, 150–154. [PubMed: 22842902]

Tashiro A, Sandler VM, Toni N, Zhao C, and Gage FH (2006a). NMDA-receptor-mediated, cell-specific integration of new neurons in adult dentate gyrus. Nature 442, 929–933. [PubMed: 16906136]

Tashiro A, Zhao C, and Gage FH (2006b). Retrovirus-mediated single-cell gene knockout technique in adult newborn neurons in vivo. Nat. Protoc. 1, 3049–3055. [PubMed: 17406567]

Tashiro A, Makino H, and Gage FH (2007). Experience-specific functional modification of the dentate gyrus through adult neurogenesis: a critical period during an immature stage. J. Neurosci. 27, 3252–3259. [PubMed: 17376985]

Toni N, and Schinder AF (2015). Maturation and functional integration of new granule cells into the adult hippocampus. Cold Spring Harb. Perspect. Biol. 8, a018903. [PubMed: 26637288]

Trinchero MF, Herrero M, Monzón-Salinas MC, and Schinder AF (2019). Experience-dependent structural plasticity of adult-born neurons in the aging hippocampus. Front. Neurosci. 13, 739. [PubMed: 31379489]

Tunc-Ozcan E, Peng CY, Zhu Y, Dunlop SR, Contractor A, and Kessler JA (2019). Activating newborn neurons suppresses depression and anxiety-like behaviors. Nat. Commun. 10, 3768. [PubMed: 31434877]

Tuncdemir SN, Lacefield CO, and Hen R (2019). Contributions of adult neurogenesis to dentate gyrus network activity and computations. Behav. Brain Res. 374, 112112. [PubMed: 31377252]

van Praag H, Kempermann G, and Gage FH (1999). Running increases cell proliferation and neurogenesis in the adult mouse dentate gyrus. Nat. Neurosci. 2, 266–270. [PubMed: 10195220]

van Praag H, Schinder AF, Christie BR, Toni N, Palmer TD, and Gage FH (2002). Functional neurogenesis in the adult hippocampus. Nature 415, 1030–1034. [PubMed: 11875571]

Vogel-Ciernia A, and Wood MA (2014). Examining object location and object recognition memory in mice. Curr. Protoc. Neurosci. 69, 8.31.1–8.31.17. [PubMed: 25297693]

Yang SM, Alvarez DD, and Schinder AF (2015). Reliable genetic labeling of adult-born dentate granule cells using Ascl1 CreERT2 and Glast CreERT2 murine lines. J. Neurosci. 35, 15379–15390. [PubMed: 26586824]

Zhao C, Teng EM, Summers RG, Ming GL, and Gage FH (2006). Distinct morphological stages of dentate granule neuron matruation in the adult mouse hippocampus. J. Neurosci 26, 3–11. [PubMed: 16399667]

Highlights

- Kainate receptors are expressed on developing adult-born dentate granule cells
- KARs in adult-born neurons affect their synaptic and intrinsic properties
- Timed ablation of KARs during a critical period disrupts spatial discrimination in mice

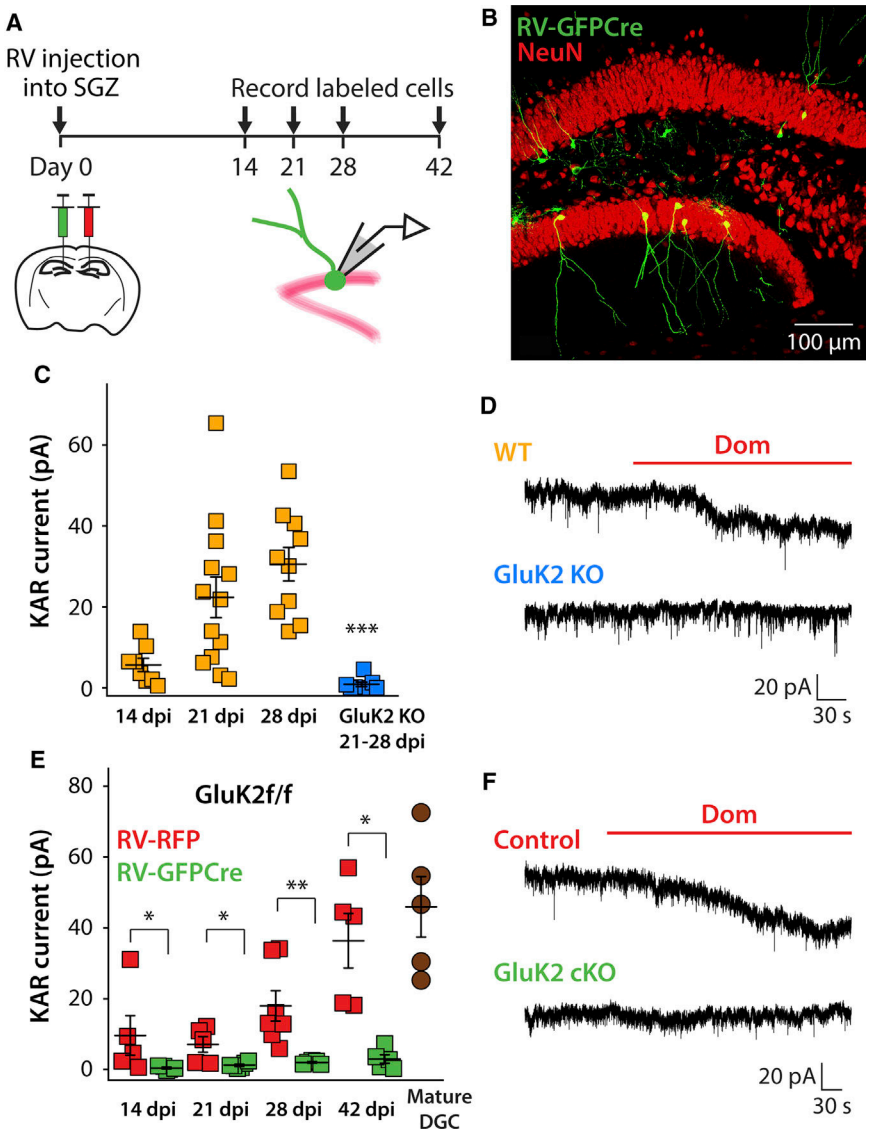

Figure 1. GluK2-containing KARs are present in young abDGCs

(A) Schematic illustration of the experimental paradigm: retrovirus carrying an RFP or GFP-IRES-Cre vector was delivered to the subgranular zone of the dentate gyrus in 8–10-week-old mice. Labeled cells were recorded at various days postinjection (dpi).

(B) Representative confocal image showing GFP-IRES-Cre-expressing (green) abDGCs from a 28 dpi *Grik2*f/f mouse. NeuN immunofluorescence is shown in red.

(C) KAR currents in abDGCs (orange) increase progressively with age (14 dpi, n = 8; 21 dpi, n = 13; 28 dpi, n = 10) but are eliminated in the GluK2 KO mouse, 21–28 dpi, n = 10, ***$p < 0.001$.

(D) Example recording traces representing domoate-induced, KAR-mediated current in a 28 dpi WT and GluK2 KO abDGC.

(E) Cre-mediated deletion of GluK2 in Grik2f/f mice results in loss of KAR-mediated current in abDGCs at all ages post injection (14 dpi, n = 5 and 5; 21 dpi, n = 5 and 6; 28 dpi, n = 7 and 5; 42 dpi, n = 5 and 5; mature DGC, n = 5).

(F) Example recordings of domoate-induced currents in a 28 dpi control and GluK2 cKO abDGC. Data are presented as means ± SEM. Statistical analysis: Mann-Whitney U test, *p < 0.05, **p < 0.01, ***p < 0.001.

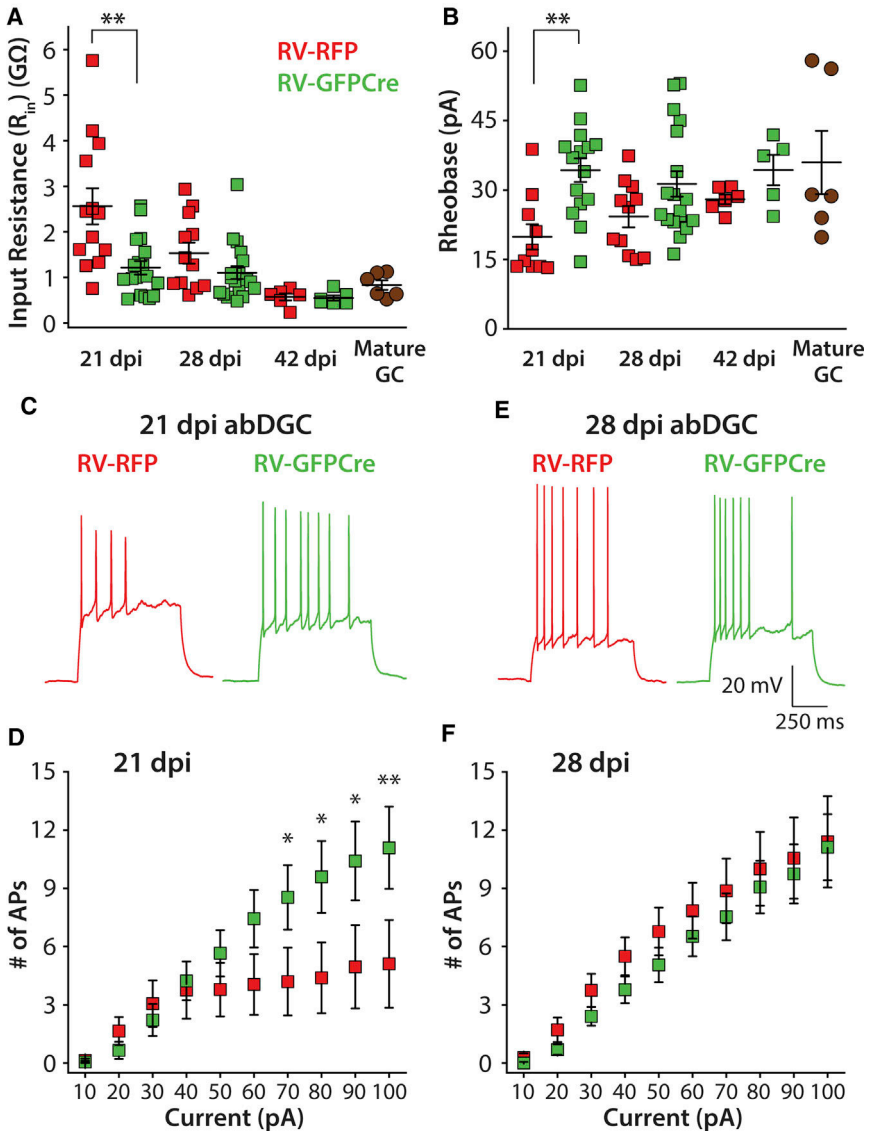

Figure 2. Development of intrinsic and AP firing properties are accelerated in 21 dpi GluK2 cKO abDGCs

(A) Input resistance (R_{in}) of developing GluK2 cKO abDGCs (RV-GFPCre) compared with control abDGCs (RV-RFP) at 21 dpi (n = 18 and 13), 28 dpi (n = 19 and 12), and 42 dpi (n = 6 and 6), and from unlabeled mature GluK2$^{+/+}$ GCs (n = 6) in *Grik2*f/f mice.

(B) Rheobase of developing GluK2 cKO abDGCs compared with controls at 21 dpi (n = 15 and 10), 28 dpi (n = 18 and 11), 42 dpi (n = 5 and 6), and mature WT GCs (n = 6). Significant differences were observed in recordings from 21 dpi abDGCs.

(C) Example AP firing profiles of 21 dpi control (RV-RFP) and cKO (RV-GFPCre) abDGCs in response to a 70 pA current injection step of 800 ms duration.

(D) AP response properties across a range of current injections in 21 dpi control and cKO abDGCs. Significant increases in number of APs were observed at current injection steps between 70 and 100 pA in 21 dpi GluK2 cKO abDGCs (RV-RFP, n = 14; RV-GFPCre, n = 16).

(E and F) Example traces and input-output AP response of 28 dpi abDGCs (RV-RFP, n = 12; RV-GFPCre, n = 18).

Statistical analysis: Mann-Whitney U test (A and B); two-way repeated-measures ANOVA (D and F); *p< 0.05, **p < 0.01.

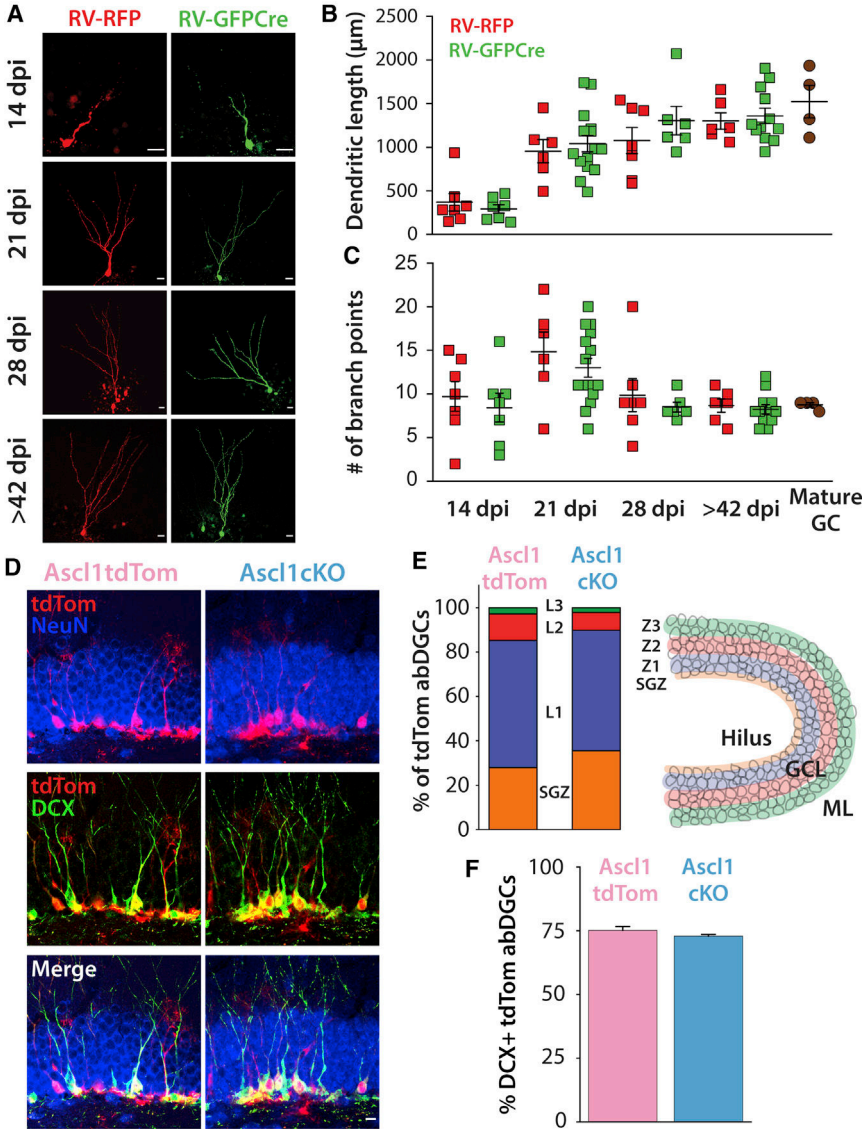

Figure 3. Morphological development of GluK2 cKO abDGCs

(A) Representative images of biocytin-filled control (RV-RFP) and cKO (RV-GFPCre) abDGCs at several postmitotic dpi stages.

(B) Total dendritic length of RV-RFP and RV-GFPCre abDGCs at each dpi (14 dpi, n = 7 and 7; 21 dpi, n = 6 and 15; 28 dpi, n = 7 and 6; >42 dpi, n = 6 and 12) and of unlabeled mature GluK2$^{+/+}$ control GCs (n = 4).

(C) Number of dendritic branch points of abDGCs at each dpi and mature GluK2$^{+/+}$ GCs.

(D) Representative images of abDGCs labeled with tdTom (red), NeuN (blue), and DCX (green) from a cohort of Ascl1tdTom (control) and Ascl1cKO (*GriK2* timed ablation) neurons. In each case, the labeled cohort is 21 days and younger.

(E) Analysis of radial migration of control and Ascl1cKO abDGCs into the granule cell layers 21 days after TAM induction (Ascl1tdTom, n = 5; Ascl1cKO, n = 3).

(F) Quantification of co-expression of DCX and tdTom in abDGCs 21 days and younger in Ascl1tdTom (control)(n = 5) and Ascl1cKO mice (n = 3).

Scale bars in (A) and (D): 15 μm. Statistical analysis: Mann-Whitney U test.

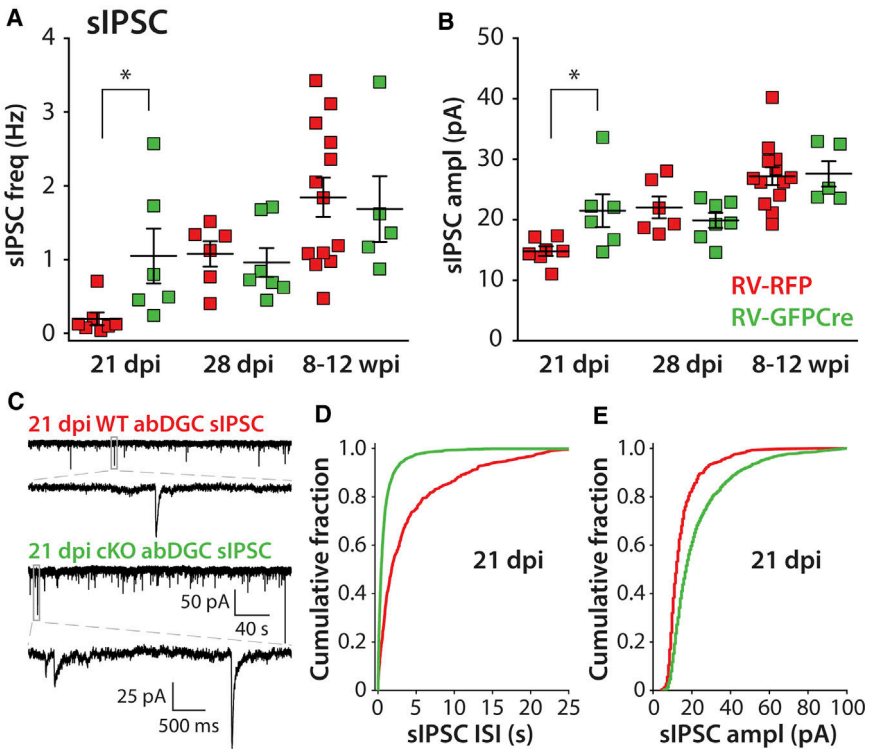

Figure 4. Development of GABAergic synapses is altered in 21 dpi GluK2 cKO abDGCs

(A and B) Average sIPSC frequency and amplitudes in GluK2 cKO abDGCs (RV-GFPCre) and control abDGCs (RV-RFP) at 21 dpi (RV-RFP, n = 7; RV-GFPCre, n = 6), 28 dpi (RV-RFP, n = 6; RV-GFPCre, n = 7), and 8–12 weeks postinjection (wpi; RV-RFP, n = 13; RV-GFPCre, n = 5).

(C) Representative current traces of sIPSC recorded from a 21 dpi control and GluK2 cKO abDGC.

(D) Cumulative fraction of all sIPSC inter-event intervals for 21 dpi GluK2 cKO (n = 6) and control abDGCs (n = 7).

(E) Cumulative fraction of all sIPSC amplitudes for 21 dpi GluK2 cKO (n = 6) and control abDGCs (n = 7).

Statistical analysis: Mann-Whitney U test; *p < 0.05.

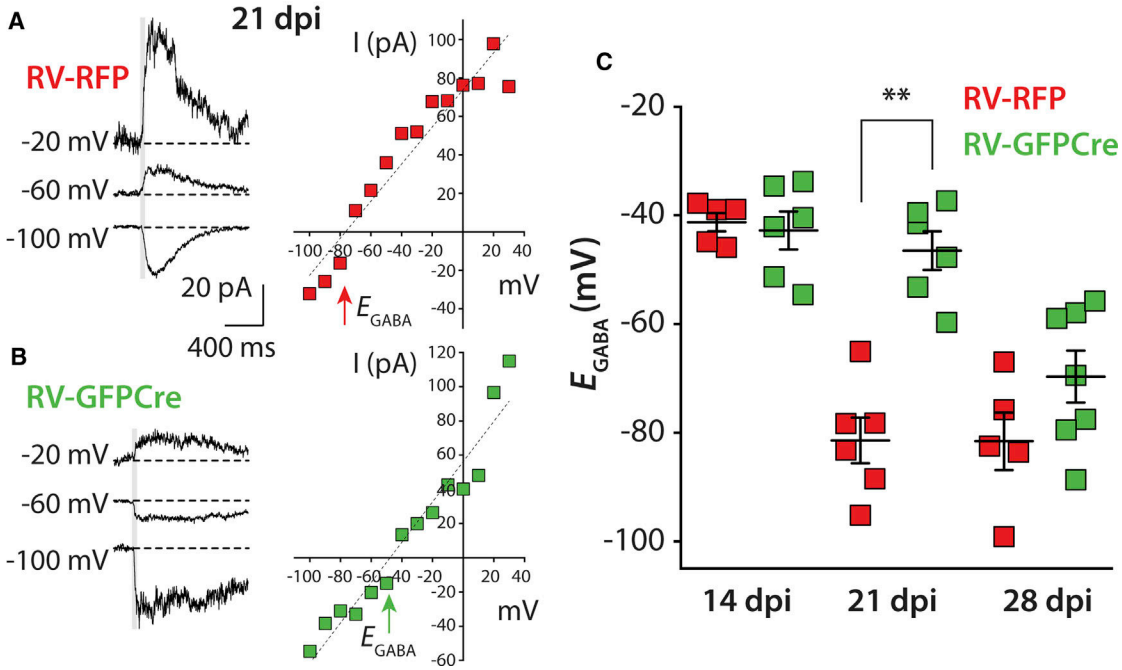

Figure 5. E_{GABA} polarity switch is disrupted in 21 dpi GluK2 cKO abDGCs

(A and B) Representative GABA-evoked currents from gramicidin-perforated patch recording and associated current-voltage relationship curves with the GABA reversal denoted from a 21 dpi control (RV-RFP) and cKO (RV-GFPCre) abDGC.

(C) Grouped data from all recordings of E_{GABA} measured in control and cKO abDGCs at 14 dpi (RV-RFP, n = 5; RV-GFPCre, n = 6), 21 dpi (RV-RFP, n = 6; RV-GFPCre, n = 6), and 28 dpi (RV-RFP, n = 5; RV-GFPCre, n = 7).

Statistical analysis: Mann-Whitney U test; **p < 0.01.

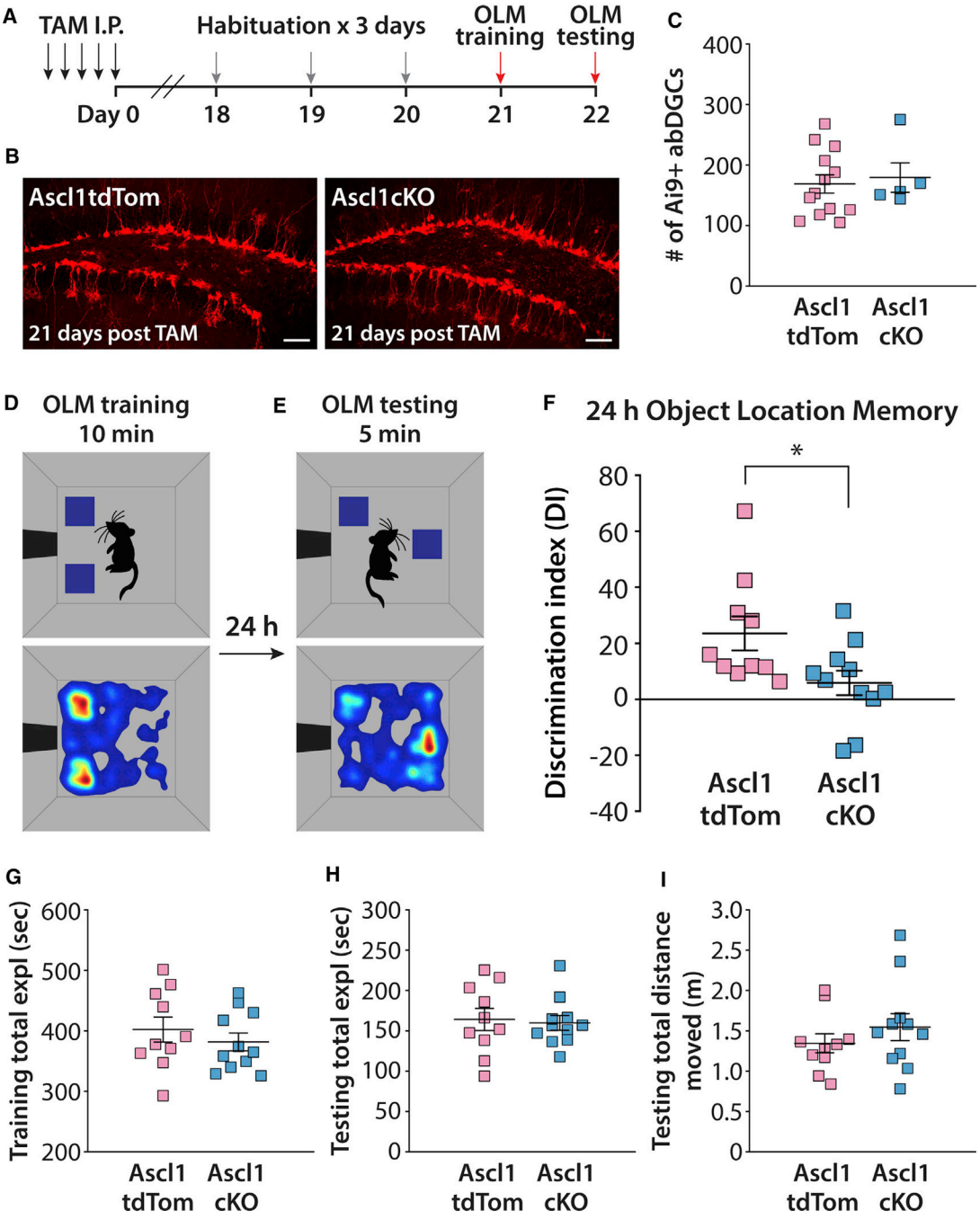

Figure 6. Spatial discrimination is impaired by cKO of GluK2 in a young cohort of abDGCs

(A) Timeline of cKO using TAM administration and object location memory task; 180 mg/kg tamoxifen was administered to 8–9-week-old *Grik2*f/f;Ai9;*Ascl1*^{CreERT2} or *Grik2*$^{+/+}$;Ai9;*Ascl1*^{CreERT2} mice via intraperitoneal (i.p.) injection.

(B) Example images of hippocampal dentate region from Ascl1tdTom (left) and Ascl1cKO (right) mice with tdTom labeled abDGCs at 21 days after TAM induction.

(C) Cell counts of labeled neurons per section (50 mm thickness) in Ascl1tdTom and Ascl1cKO mice.

(D and E) Schematic of OLM training (D) (top) and OLM testing (E) (top) and representative heatmaps of mouse position during each session (bottom).
(F) Calculated discrimination index from all experiments, reflecting preference for novel object location of Ascl1tdTom (n = 10) and Ascl1cKO mice (n = 11) 22 days after TAM induction.
(G and H) Total exploration time of mice for both object locations during OLM training phase and OLM testing phase.
(I) Total distance Ascl1tdTom and Ascl1cKO mice moved during OLM testing.
Statistical analysis: Mann-Whitney U test; *$p < 0.05$.

KEY RESOURCES TABLE

REAGENT or RESOURCE	SOURCE	IDENTIFIER
Antibodies		
Rabbit polyclonal anti-RFP	Abcam	Cat#ab62341; RRID: AB_945213
Goat polyclonal anti-doublecortin (C-18)	Santa Cruz Biotechnology	Cat#sc-8066; RRID: AB_2088494
Chicken polyclonal anti-NeuN	Millipore	Cat#ABN91; RRID: AB_11205760
Donkey anti-Rabbit IgG (H+L) highly crossadsorbed secondary antibody, Alexa Fluor Plus 594	Thermo Fisher Scientific	Cat#A32754; RRID: AB_2762827
Donkey anti-Goat IgG (H+L) highly crossadsorbed secondary antibody, Alexa Fluor Plus 680	Thermo Fisher Scientific	Cat#A32860; RRID: AB_2762841
Donkey anti-Chicken IgY polyclonal antibody, biotin conjugated	Millipore	Cat#AP194B; RRID: AB_92675
Streptavidin, Alexa Fluor 488 conjugate antibody	Molecular Probes	Cat#S32354; RRID: AB_2315383
Streptavidin, Alexa Fluor® 555 conjugate antibody	Thermo Fisher Scientific	Cat#S32355; RRID: AB_2571525
Streptavidin, Alexa Fluor 405 conjugate antibody	Thermo Fisher Scientific	Cat#S32351
Donkey anti-Rabbit IgG(H+L)-UNLB antibody	SouthernBiotech	Cat#6441–01; RRID: AB_2796371
Donkey anti-Chicken IgY (H+L) secondary antibody	Thermo Fisher Scientific	Cat#SA1–72002; RRID: AB_923387
Donkey anti-Goat IgG Fc-UNLB antibody	SouthernBiotech	Cat#6460–01; RRID: AB_2796393
Bacterial and virus strains		
CAG-RFP retrovirus	This paper	N/A
CAG-GFP retrovirus	This paper	N/A
CAG-GFP-IRES-CRE retrovirus	This paper	N/A
Chemicals, peptides, and recombinant proteins		
Tetrodotoxin	Tocris	Cat#1078; CAS: 4368–28–9
Tamoxifen	Sigma-Aldrich	Cat#T5648; CAS: 10540–29–1
Domoate	Sigma-Aldrich	Cat#D6152; CAS: 14277–97–5
Bicuculline	Sigma-Aldrich	Cat#14340; CAS: 485–49–4
Picrotoxin	Abcam	Cat#ab120315; CAS: 124–87–8
GYKI 52466 dihydrochloride	Tocris	Cat#1454; CAS: 2319722–40–0
D-APV	Alomone Labs	Cat#D-145; CAS: 79055–68–8
CNQX	Alomone Labs	Cat#C-141; CAS: 479347–85–8
GABA	Sigma-Aldrich	Cat#A2129; CAS: 56–12–2
Gramacidin	Sigma-Aldrich	Cat#G5002; CAS: 1405–97–6
Biocytin	Sigma-Aldrich	Cat#B4261; CAS: 576–19–2
Lipofectamine 2000 transfection reagent	Thermo Fisher Scientific	Cat#11668019
Opti-MEM reduced serum medium	Thermo Fisher Scientific	Cat#31985070
Experimental models: Cell lines		
GP2–293 cell line	Laboratory of John Kessler	RRID: CVCL_WI48

REAGENT or RESOURCE	SOURCE	IDENTIFIER
Experimental models: Organisms/strains		
Mouse: GluK2 KO: GluR6$^{-/-}$	Mulle et al., 1998	N/A
Mouse: Ascl1^{CreERT2};*Grik2*f/f;Ai9: *Ascl1*$^{tm1.1(Cre/ERT2)Jejo}$/J;*Grik2*f/f;B6.Cg-*Gt(ROSA)26Sor*$^{tm9(CAG–tdTomato)Hze}$/J	The Jackson Laboratory; Marshall et al., 2018	N/A
Oligonucleotides		
Ascl1^{CreERT2} forward primer (10843): 5' AACTTTCCTCCGGGGCTCGTTTC 3'	Integrated DNA Technologies	N/A
Ascl1^{CreERT2} reverse primer (10653): 5' CGCCTGGCGATCCCTGAACAT G 3'	Integrated DNA Technologies	N/A
Ai9 forward primer (oIMR9105): 5' CTGTTCCTGTACGGCATGG 3'	Integrated DNA Technologies	N/A
Ai9 reverse primer (oIMR9103): 5' GGCATTAAAGCAGCGTATCC 3'	Integrated DNA Technologies	N/A
*Grik2*f/f forward primer (132): 5' TCCTAAATAAAACTGATGAAGAG 3'	Integrated DNA Technologies	N/A
*Grik2*f/f reverse primer (133): 5' CGTAGCTAAATTTAAAAGTGAACA 3'	Integrated DNA Technologies	N/A
GluK2 KO forward primer (402): 5' GTGAGACGTGCTACTTCCATTTG 3'	Integrated DNA Technologies	N/A
GluK2 KO reverse primer (860): 5' CAGGGTTGCAAGGGTGTGG 3'	Integrated DNA Technologies	N/A
Recombinant DNA		
Plasmid: CAG-RFP	Tashiro et al., 2006a	N/A
Plasmid: CAG-GFP	Zhao et al., 2006	RRID: Addgene_16664
Plasmid: CAG-GFP-IRES-CRE	Zhao et al., 2006	RRID: Addgene_48201
Plasmid: VSV-G	Laboratory of John Kessler	N/A
Software and algorithms		
ImageJ	Schneider et al., 2012	RRID:SCR_003070
Imaris	Bitplane	RRID: SCR_007370
Mini Analysis Program	Synaptosoft Inc.	RRID: SCR_002184
EthoVision XT	Noldus	RRID: SCR_000441
FreezeFrame 4	Actimetrics	RRID: SCR_014429
pClamp 10 software suite	Molecular Devices	RRID: SCR_011323